
1 **Evaporation and sublimation measurement and modelling of an alpine saline lake influenced by**
2 **freeze–thaw on the Qinghai–Tibet Plateau**

3 Fangzhong Shi^{1,2}, Xiaoyan Li^{1,2,3,4}, Shaojie Zhao^{1,2}, Yujun Ma⁵, Junqi Wei^{1,2}, Qiwen Liao^{1,2}, Deliang
4 Chen⁶

5 ¹State Key Laboratory of Earth Surface Processes and Resource Ecology, Faculty of Geographical
6 Science, Beijing Normal University, Beijing 100875, China;

7 ²School of Natural Resources, Faculty of Geographical Science, Beijing Normal University, Beijing
8 100875, China

9 ³Key Laboratory of Tibetan Plateau Land Surface Processes and Ecological Conservation, Ministry of
10 Education, Qinghai Normal University, Xining, China

11 ⁴Academy of Plateau Science and Sustainability, Qinghai Normal University, Xining, China

12 ⁵School of Geography and Planning, Sun Yat–sen University, Guangzhou, China

13 ⁶Regional Climate Group, Department of Earth Sciences, University of Gothenburg, Gothenburg,
14 Sweden.

15 * To whom the correspondence should be addressed: Xiao–Yan Li, State Key Laboratory of Earth
16 Surface Processes and Resource Ecology, Beijing Normal University, Beijing, China. Emails:
17 xyli@bnu.edu.cn.

18 ✉ Fangzhong Shi (during review) fzshi@mail.bnu.edu.cn

19 ✉ Xiaoyan Li* (after acceptance) xyli@bnu.edu.cn

20

21

22

23 **Key Points**

24 ● Night evaporation of Qinghai Lake accounts for more than 40% of the daily evaporation during
25 both the ice-free and ice-covered periods.

26 ● Lake ice sublimation reaches 175.22 ± 45.98 mm, accounting for 23% of the annual evaporation.

27 ● Wind speed weakening may have resulted in an ~~11.44~~17.56% decrease in lake evaporation
28 during the ice-covered period from 2003 to 2017.

29 **Abstract**

30 Saline lakes on the Qinghai–Tibet Plateau (QTP) ~~profoundly~~ affect the regional climate and water cycle
31 through ~~water loss-of water~~ (E, evaporation under ice-free ~~(IF)~~ and sublimation under ice-covered ~~(IC)~~
32 conditions). Due to the observation difficulty over lakes, E and its underlying driving forces are seldom
33 studied targeting saline lakes on the QTP, particularly during the ~~ice-covered IC~~ periods (ICP). In this
34 study, ~~The~~ E of Qinghai Lake (QHL) and its influencing factors during the ~~ice-free periods~~ (IFP) and
35 ICP were first quantified based on six years of observations. Subsequently, ~~two-three~~ models were
36 ~~calibrated~~ ~~chosen~~ and ~~compared~~ ~~applied~~ in simulating E ~~and its response to climate variation~~ during the
37 IFP and ICP from 2003 to 2017. The annual E sum of QHL is 768.58 ± 28.73 mm, and ~~the~~ E sum during
38 the ICP reaches 175.22 ± 45.98 mm, accounting for 23% of the annual E sum. ~~The~~ E is mainly controlled
39 by the wind speed, vapor pressure difference, and air pressure during the IFP, but ~~is~~ driven by the net
40 radiation, the difference between the air and lake surface temperatures, wind speed, and ice coverage
41 during the ICP. The mass transfer model simulates lake E well during the IFP, and the model based on
42 energy achieves a good simulation during the ICP. Moreover, wind speed weakening ~~results~~ ~~resulted~~ in
43 an ~~11.147.56~~% decrease in E during the ICP of 2003–2017. Our results highlight the importance of E in
44 ICP, provide new insights into saline lake E in alpine regions, and can be used as a reference to further
45 improve hydrological models of alpine lakes.

46 **Keywords:**

47 Lake evaporation and sublimation, saline lakes, flux observation, ice-covered periods, Qinghai Lake,
48 Qinghai–Tibet Plateau

49 1. Introduction

50 Saline lakes account for 23% of the total area and 44% of the total water volume of Earth's lakes
51 (Wurtsbaugh et al., 2017). They ~~are critical~~~~play an important role~~ in shaping the regional climate and
52 maintaining ecological security and sustainable development in arid regions (Messenger et al., 2016;
53 Wurtsbaugh et al., 2017; Woolway et al., 2020; Wu et al., 2021; Wu et al., 2022). Under the influences
54 of climate change and human activities, saline lakes worldwide have changed rapidly in terms of their
55 area, level, temperature, ice phenology, energy and water exchange, which has become an issue of
56 concern (Gross, 2017; Wurtsbaugh et al., 2017; Woolway et al., 2020). Evaporation under ice-free
57 ~~periods (IFP) and sublimation under ice-covered (IC) periods (ICP) (E) is are an~~ important mechanisms
58 of ~~the~~ transfer of energy and water between lakes and ~~the~~ atmosphere, and ~~are amongis one of the main~~
59 ~~major~~ factors influencing changes in ~~the~~ lake water volume (~~Lazhu et al., 2016~~; Ma et al., 2016; ~~Zhu et~~
60 ~~al., 2016~~; Woolway et al., 2018; Guo et al., 2019; Woolway et al., 2020).

61 In contrast to freshwater lakes, E (~~evaporation under IFP and sublimation under ICP~~) of saline lakes
62 involves a more complex process and is affected not only by climate conditions, ~~lake depth, temperature,~~
63 ~~stratification, thermal stability and hydrodynamics,~~ but also by ~~the salinity, lake depth, temperature,~~
64 ~~stratification, thermal stability, and hydrodynamics~~ (Salhotra et al., 1985; Hamdani et al., 2018; Obianyo,
65 2019; Woolway et al., 2020). For example, dissolved salt ions can reduce the free energy of water
66 molecules (i.e., reduce~~d~~ water activity) and result in a reduced saturated vapor pressure above saline
67 lakes at a given water temperature (Salhotra et al., 1987; Mor et al., 2018). Previous studies have
68 investigated the relationship between ~~the~~ E and salinity of saline lakes and discrepancies in the
69 controlling factors between different time scales (Salhotra et al., 1987; Lensky et al., 2018; Hamdani et
70 al., 2018; Mor et al., 2018). These studies have mainly focused on saline lakes in arid and temperate
71 zones, and the interaction and mutual feedback between the water body of saline lakes and the
72 atmosphere remain unclear. ~~In particular, t~~here are few studies on ~~the~~ E of alpine saline lakes ~~which~~
73 ~~that~~ exhibit complex hydrology and limnology.

74 Saline lakes account for over 70% of the total lake area on the Qinghai-Tibet Plateau (QTP) (Liu et al.,
75 2021), and thus profoundly affect the regional climate and water cycle through ~~the~~ E (Yang et al., 2021).
76 However, continuous year-round direct measurements of saline lake E are scarce, which hinders the

77 exploration of lake E at different time scales. Observations of E from saline lakes have been obtained for
78 Qinghai Lake (QHL) (Li et al., 2016), Namco (Wang et al., 2015; Ma et al., 2016), Selinco (Guo et al.,
79 2016), and Erhai (Liu et al., 2015) via the eddy–covariance (EC) technique or pan E on the QTP, but
80 these observations are mainly ~~for during the growing seasons~~IFP (or IF: approximately mid–May to mid–
81 October). Thus, there are considerably fewer E observations during the ICP and full–year period of lakes,
82 ~~mainly mostly~~ because of the harsh environment and limited accessibility to the QTP (Lazhu-Zhu et al.,
83 2016). However, most lakes on the QTP exhibit a long and stable ICP lasting more than 100 days due to
84 the low annual air temperature (Ta) (Cai et al., 2019), which suggests that E observations are currently
85 lacking for nearly a quarter of the year (from the IFP to the ICP). Although studies have commented on
86 the importance of E during the ICP (Li et al., 2016; Wang et al., 2020) and clarified that freezing/breakup
87 processes could result in sudden changes in lake surface properties (such as albedo and roughness) and
88 affect the water and energy exchange between the lake and atmosphere (Cai et al., 2019; Yang et al.,
89 2021), the dynamic processes of energy interchange and E of saline lakes during the ICP and its responses
90 to ~~climatic variability, climate warming~~ on the QTP still constitute a knowledge gap in lake hydrology
91 research. Thus, there is an urgent need to better quantify lake E during the ICP on the QTP.

92 ~~A large number of~~Many models have been employed to calculate lake E, mainly including the Dalton
93 formula series based on mass transfer and aerodynamics, energy and water balance formula series,
94 Penman formula series considering both aerodynamics and energy balance, and empirical formulas based
95 on statistical analysis (Dalton, 1802; Bowen, 1926; Penman, 1948; Harbeck et al., 1958; Finch and Calver,
96 2008; Hamdani et al., 2018; Wang et al., 2019a). However, the reported values exhibit large discrepancies
97 in their seasonal variations and annual amounts between those models (Lazhu-Zhu et al., 2016; Ma et al.,
98 2016; Guo et al., 2019; Wang et al., 2019a; Wang et al., 2020), and almost all models were calibrated
99 and verified against E observations during the IFP ~~as a result of the deficiency in observed E during the~~
100 ~~IC~~ (Lazhu et al., 2016; Guo et al., 2019), and ~~while~~ E during the ICP was either not calculated or
101 unverified (Wang et al., 2020), ~~as a result of the deficiency in observed E during the ICP~~ (Zhu et al., 2016;
102 Guo et al., 2019). In addition, compared with small lakes, large and deep lakes exhibit higher E levels
103 and delayed seasonal E peaks because more energy is absorbed and stored in large and deep lakes during
104 the IFP and released during the ICP (Wang et al., 2019a). Thus, the effect of changes in ice phenology on
105 lake E is particularly important, which calls for different models for E simulation during the IFP and ICP.

106 Furthermore, with increasing overall surface air warming and moistening, solar dimming, and wind
107 stilling since the beginning of the 1980s (Yang et al., 2014), lakes on the QTP have experienced a
108 significant temperature increase (at a rate of 0.037°C/yr from 2001 to 2015) (Wan et al., 2018) – and ice
109 phenology shortening (at a rate of –0.73 d/yr from 2001 to 2017) (Cai et al., 2019). Changes in ~~the air~~
110 T_a , water surface temperature (T_s), wind speed (WS), and ice phenology could impose different effects
111 on energy interchange and molecular diffusion due to differences in the state phase and reflectance of
112 water between the ICP and IFP, thus altering lake E (Wang et al., 2018). Although many studies have
113 reported a decrease in ~~lake E of lakes~~ on the QTP by model simulations (Lazhu et al., 2016; Ma et al.,
114 2016; Zhu et al., 2016; Li et al., 2017; Guo et al., 2019), owing to E neglect during the ICP, the potential
115 mechanisms of lake E and its different responses to ~~elimate change climate variability~~ during the ICP and
116 IFP remain unclear.

117 In this study, based on six continuous years of direct measurements of lake E and energy exchange flux
118 data obtained with the EC technique pertaining to QHL, the largest saline lake on the QTP, between 2014
119 and 2019, we quantified the characteristics of energy interchange and E on diurnal, seasonal (IFP, ICP
120 and cycle year: AN) and yearly time scales and identified the potential ~~factors influencing~~
121 ~~factors of~~ E during the IFP and ICP. In addition, combined with reanalysis climate datasets, a mass
122 transfer model (MT model), ~~an atmospheric dynamics model (AD model)~~, and a model based on energy,
123 temperature and WS (JH model) were calibrated and verified, with the optimal model chosen for the
124 simulation of lake E and its response to ~~elimate-climatic variability change~~ during the IFP and ICP from
125 2003 to 2017. The results ~~would~~ highlight the importance and potential mechanisms of E during ICP, and
126 can be used as a reference to further improve hydrological models of alpine lakes.

127 2. Materials and Methods

128 2.1. ~~Study areaite description and energy exchange flux and climate data~~

129 QHL (36°32'–37°15' N, 99°36'–100°47' E, 3194 m a.s.l.), with an area of 4,432 km² and a catchment
130 of 29,661 km², is the largest inland saline lake in China (Li et al., 2016). The average depth of the lake
131 is 26 m. The average salt content is 14.13 g L⁻¹, and the pH ranges from 9.15 to 9.30. The hydrochemical
132 type of the lake water is Na–SO₄–Cl (Li et al., 2016). ~~Surrounded by mountains, the QHL is a typical~~

133 closed tectonic depression lake, which is fed by five major rivers, including the Buha, Shaliu, Hargai,
134 QuANJI, and Heima Rivers (Jin et al., 2015). The total annual water discharge is approximately 1.56×10^9
135 m^3 , of which the Buha River contributes 50% and Shaliu River contributes approximately one third (Jin
136 et al., 2015). The mean annual T_a , precipitation, and E values between 1960 and 2015 were $-0.1^\circ C$, 355
137 mm and 925 mm, respectively (Li et al., 2016). The seasonal stratification of QHL corresponded to that
138 of a dimictic lake with the spring overturn taking place around May and the autumn overturn appearing
139 around November–December (Su et al., 2019). The ICP usually begins in late November, ends in mid–
140 late March or even early April, and lasts more than 100 days. Under the effects of climate warming, QHL
141 has experienced temperature increases, area expansion, and ICP shortening in the last two decades (Tang
142 et al., 2018; Han et al., 2021).

143 **2.2. Site description and energy exchange flux and climate data**

144 The instruments to measure the energy exchange flux and micrometeorological parameters were installed
145 at the China Torpedo Qinghai Lake test base ($36^\circ 35' 27.65'' N$, $100^\circ 30' 06'' E$, 3198 m a.s.l.) located in
146 the southeastern QHL approximately 737 m from the nearest shore (Li et al., 2016) (Fig. 1). The water
147 depth underneath this platform is 18 m. The torpedo test tower has a height of 10 m above the water
148 surface. The EC system was installed on a steel pillar mounted on the northwestern side of the top of the
149 torpedo test tower with a total height of 17.3 m above the lake water surface (Li et al., 2016). A three–
150 dimensional sonic anemometer (model CSAT3, Campbell Scientific Inc., Logan, UT, USA) was used to
151 directly measure horizontal and vertical wind velocity components (u , v , and w) and virtual temperature.
152 An open–path infrared gas analyzer (model EC150, Campbell Scientific Inc.) was applied to measure
153 fluctuations in water vapor and carbon dioxide concentrations. Fluxes of sensible heat (H) and latent heat
154 (LE) were calculated from the 10–Hz time series at 30–min intervals and recorded by a data logger
155 (CR3000, Campbell Scientific Inc.). The observation instruments were powered by solar energy.

156 A suite of auxiliary micrometeorology was also measured as 30–min averages of 1–s readings on the
157 eastern side of the top of the torpedo test tower, 3 m away from the EC instruments. The net radiation
158 (R_n) was calculated from the incoming shortwave, reflected shortwave, and incoming and outgoing
159 longwave radiation, which were measured by a net radiometer (CNR4, Kipp & Zonen B.V., Delft,
160 Netherlands) at 10 m above the lake surface (Fig. 1; Table S1). The T_a , relative humidity (RH) and air

设置了格式: 上标

设置了格式: 上标

带格式的: 标题 3

161 pressure (Pres) were measured at a height of 12.5 m above the water surface (Table S1). A wind sentry
162 unit (model 05103, RM Young, Inc. Traverse City, MI, USA) was employed to measure the WS and wind
163 direction (WD) (Table S1). The Ts was measured with an infrared thermometer (model SI-111, Campbell
164 Scientific Inc.) approximately 10 m above the water surface, and the water temperature (Tl) was
165 measured with five temperature probes (109 L, Campbell Scientific Inc.) at depths of 0.2, 0.5, 1.0, 2.0
166 and 3.0 m. Precipitation was measured with an automated tipping-bucket rain gauge (model TE525,
167 Campbell Scientific Inc.) and precipitation gauge (model T-200B, Campbell Scientific Inc.) (Table S1).
168 The observation system began operation on May 11, 2013. In this study, we unified all observational data
169 at 30-min intervals and analyzed the data from January 1, 2014 to December 31, 2019 (Table S1).

170 2.23. Reanalysis climate datasets

171 The reanalysis climate datasets used to drive the lake E models were acquired from the interim reanalysis
172 dataset v5 (ERA5) produced by the European Centre for Medium-Range Weather Forecasts
173 (<https://cds.climate.copernicus.eu/cdsapp#!/search?type=dataset>) and the China Regional High-
174 Temporal-Resolution Surface Meteorological Elements-Driven Dataset (CMFD)
175 (<http://data.tpdc.ac.cn/en/>). Gridded hourly ERA5 skin temperature and daily WS, daily CMFD Ta, Pres,
176 RH, and downward shortwave radiation (Rs) at a spatial resolution of 0.1° from 2001 to 2018 were
177 analyzed in this study (Table S1). The daily skin temperature was generated by averaging the hourly
178 temperature over 24 h per day and was adopted as the lake surface temperature. We extracted climate
179 data pertaining to QHL via a grid mask with a spatial resolution of 0.1° and averaged the data in all pixels.
180 Considering the advantages of long-time spans and high resolution, the ERA5 and CMFD datasets
181 developed based on land station data have been recognized as the best currently available reanalysis
182 products and have been widely applied in land-surface and hydrological modeling studies in China
183 (Lazhu et al., 2016; Ma et al., 2016; Zhu et al., 2016; Tian et al., 2021; Xiao and Cui, 2021). To reduce
184 the uncertainty caused by the input data, the daily lake surface temperature and WS from ERA5, Ta and
185 Rs, RH and Pres from CMFD for QHL were adjusted with fitting equations of the observed daily Ts (R^2
186 = 0.92, $P < 0.01$), Ta ($R^2 = 0.90$, $P < 0.01$), and Rs ($R^2 = 0.73$, $P < 0.01$), WS ($R^2 = 0.55$, $P < 0.01$), RH
187 ($R^2 = 0.63$, $P < 0.01$) and Pres ($R^2 = 0.95$, $P < 0.01$)—from 2014 to 2018 (Fig. S1), and the equations
188 were shown as below:

带格式的: 制表位: 20 字符, 居中 + 38 字符, 右对齐

189 $T_a^{ad} = 1.01 \times T_a^{CMFD} + 0.71$
190 (1)

191 $T_s^{ad} = 0.71 \times T_s^{ERA5} + 3.30$ (2)

192 $R_s^{ad} = 0.86 \times R_s^{CMFD} + 34.63$
193 (3)

194 $WS_a^{ad} = 0.60 \times WS_a^{ERA5} + 0.76$ (4)

195 $RH_a^{ad} = 0.68 \times RH_a^{CMFD} + 19.95$ (5)

196 $Pres_a^{ad} = 0.97 \times Pres_a^{CMFD} + 30.72$ (6)

197 where T_a^{ad} , T_s^{ad} and R_s^{ad} , R_s^{ad} , WS_a^{ad} , RH_a^{ad} and $Pres_a^{ad}$ are T_a , T_s and R_s , WS , RH and $Pres$ of
198 ERA5 and CMFD, respectively, after adjustment, respectively.

199 **2.34. Lake ice coverage dataset and ice phenology**

200 The daily lake ice coverage of QHL from 2002 to 2018 was extracted from a lake ice coverage dataset
201 of 308 lakes (with an area greater than 3 km²) on the QTP retrieved from the National Tibetan Plateau
202 Data Center (<https://doi.org/10.11922/sciencedb.744http://data.tpdc.ac.cn/en/>). The dataset with a time
203 span from 2002 to 2018 was generated from the Moderate Resolution Imaging Spectroradiometer
204 (MODIS) normalized difference snow index (NDSI, with a spatial resolution of 500 m) product with the
205 SNOWMAP algorithm, and the data under cloud cover conditions were redetermined based on the
206 temporal and spatial continuity of lake surface conditions (Qiu et al., 2019). Based on the lake ice
207 coverage, the IFP was defined as an ice coverage lower than 10%, and the ICP was defined as an ice
208 coverage higher than 10% (Qiu et al., 2019). The ICP was divided into three stages: freeze (FZ: 10% <
209 ice coverage < 90%), completely freeze (CF: ice coverage > 90%) and thaw (TW: 10% < ice coverage <
210 90%) (Qiu et al., 2019; Qiu et al., 2019). We defined the cycle year (annual: AN) from the beginning of
211 the IFP to the end of the ICP. This ice coverage has been compared with that from two other datasets
212 based on passive microwave, and was found to be highly consistent with each other at an average R² of
213 0.86 and an RMSE of 0.13 in QHL (Qiu et al., 2019). Thus, this dataset is very accurate and suitable for
214 the division of lake ice phenology in QHL.

设置了格式: 上标

215 2.4.5 Data processing of the observed energy exchange flux and climate data

216 The EC fluxes were processed and corrected based on the 10-Hz raw time series data in the data
217 processing software EdiRe, including spike removal, lag correction of water to carbon dioxide relative
218 to the vertical wind component, sonic virtual temperature correction, performance of planar fit coordinate
219 rotation, density fluctuation correction (WPL correction) and frequency response correction (Li et al.,
220 2016). Since the shortest distance between the Chinese torpedo Qinghai Lake test base and the
221 southwestern lakeshore is only 737 m, there may be insufficient fetch for a turbulent flux under certain
222 conditions. Therefore, footprint analysis was conducted to eliminate data influenced by the surrounding
223 land. For further details on the process and results of the footprint analysis, see Li et al. (2016). In addition
224 to these processing steps, quality control of the 30-min flux data was conducted using a five-step
225 procedure: (i) data originating from periods of sensor malfunction were rejected (e.g., when there was a
226 faulty diagnostic signal), (ii) data within 1 h before or after precipitation were rejected, (iii) incomplete
227 30-min data were rejected when the missing data constituted more than 3% of the 30-min raw record,
228 (iv) data were rejected at night when the friction velocity was below 0.1 m/s (Blanken et al., 1998) and
229 (v) data with large footprints (>700 m) and a wind direction from 180° to 245° were eliminated.

230 To further control the quality of the energy exchange flux (sensible heat flux and latent heat flux: H and
231 LE, respectively) and micrometeorological dataset (Rn, Ta, Ts, Tl, RH, WS, Pres, and albedo), data
232 outside the mean $\pm 3 \times$ standard deviation were removed for each variable. Then, gap-filling methods
233 entailing a look-up table and mean diurnal variation (Falge et al., 2001) were adopted to fill gaps in the
234 flux measurement data. The look-up table method was applied when the meteorological dataset was
235 available synchronously. Otherwise, the mean diurnal variation method was adopted. The heat storage
236 change (G, W/m²) was estimated as a residual of the energy balance:

$$237 \quad \quad \quad G = R_n - LE - H$$

238 (47)

239 where Rn is the net radiation (W/m²), H is the sensible heat flux (W/m²) and LE is the latent heat flux
240 (W/m²). Lake E was calculated as

$$241 \quad \quad \quad E = \lambda \times LE$$

242 (58)

带格式的: 制表位: 20 字符, 居中 + 38 字符, 右对
齐

带格式的: 制表位: 20 字符, 居中 + 38 字符, 右对
齐

243 where λ is the latent heat of vaporization (MJ/kg), taken as 2.45 MJ/kg in this paper (Allen et al.,
244 1998).

245 **2.56. Models for daily lake evaporation simulation**

246 To evaluate the interannual variation in QHL E from 2003 to 2017, we validated three models during the
247 AN, IFP, and IC periods. Considering that Qinghai Lake is a saline lake, and many studies have pointed
248 out that it is valuable to consider the influence of salinity on saline lake evaporation, and with the increase
249 of salinity, it will exert greater inhibition on evaporation (Hamdani et al., 2018; Mor et al., 2018). Thus,
250 the water activity coefficient (α) which is defined as the ratio between the vapor pressure above saline
251 water and that above freshwater at the same temperature, has been introduced to characterize the effect
252 of salinity on saline lake evaporation (Salhotra et al., 1987; Lensky et al., 2018). Because saline water
253 drains out salt during freezing (Badawy, 2016), we only introduced the α into the evaporation simulation
254 of Qinghai Lake during IFP. The three models were as follows:

255 1) Mass-transfer model (MT model) (Harbeck et al., 1958)

256
$$E_{MT} = N \times F(WS) \times \Delta e$$

257 (69)

258
$$F(WS) = a_1 \times WS + a_2$$
 (10)(7)

259
$$\Delta e = \begin{cases} \alpha \times e_s - RH \times e_a & \text{During IFP} \\ e_s - RH \times e_a & \text{During ICP} \end{cases} \alpha \times e_s - e_a$$

260 (11)(8)

261
$$e_s = 6.105 \times \exp\left(\frac{17.27 \times T_s}{T_s + 237.7}\right)$$

262 (9)(12)

263
$$e_a = 6.105 \times \exp\left(\frac{17.27 \times T_a}{T_a + 237.7}\right)$$

264 (10)(13)

265 where E_{MT} is the E rate (mm/day); N is the mass-transfer coefficient; WS is the wind speed (m/s); Δe
266 is the vapor pressure difference and α is the water activity coefficient for saline lakes, which represents
267 the ratio between the vapor pressure above saline water and that above freshwater at the same temperature;

- 设置了格式: 字体: 10 磅

带格式的: 制表位: 20 字符, 居中 + 38 字符, 右对齐

268 and an α value of 0.97 was suggested for QHL, as measured with a portable water activity meter
 269 (AwTester, China). Moreover, e_s and e_a are the saturated vapor pressures at the lake surface
 270 temperature (T_s) and air temperature (T_a), respectively. And an α value of 0.97 was suggested for QHL
 271 during IFP, as measured with a portable water activity meter (AwTester, China). This model inherently
 272 accounts for the water salinity through Δe and requires calibration of coefficients N , a_1 and a_2 , which
 273 were taken as 1.8626, 0.0404, and 0.4317, respectively, during the AN; 0.4841, 0.4017, and 0.2628,
 274 respectively, during the IFP; and 0.9790, 0.0918, and 0.3828, respectively, during the ICP in this
 275 paper study.

276 2) Atmospheric dynamics model (AD model) (Hamdani et al., 2018)

277
$$E_{AD} = \frac{0.622 \times C_e}{\rho_w \times P} \times \rho_a \times WS \times 3.6 \times 10^6 \times \Delta e$$

 278 (4414)

279
$$\rho_a = 1.293 \times \left(\frac{273.15}{273.15 + T_a} \right) \times \frac{Pres}{101.325}$$

 280 (4215)

281 where ρ_w and ρ_a denote the water and air densities (kg/m^3), respectively, and ρ_w is approximately
 282 1.011×10^3 for QHL. Moreover, $Pres$ is the air pressure (mbar), and C_e is a transport coefficient
 283 obtained via calibration to address missing friction velocity values in the reanalysis climate datasets,
 284 which was taken as 3.2410×10^{-3} , 3.0080×10^{-3} and 6.6840×10^{-3} during the AN, IFP and ICP,
 285 respectively, in this paper.

286 3) Statistical model based on solar radiation (the Jensen–Haise method: JH model) (Wang et al., 2019a)

287
$$E_{JH} = JH1 \times (JH2 \times (T_a - T_s) + JH3) \times (R_s) \times (WS)$$

 288 (4316)

289 where R_s is the incoming solar shortwave radiation (W/m^2); $JH1$, $JH2$ and $JH3$ must be calibrated and
 290 were taken as 0.06 , -62.8020×10^{-3} , -0.01 and 5.03×10^{-3} , 0.38 , respectively, during the AN; 0.9308 ,
 291 -3.8200×10^{-3} and 0.0804 , respectively, during the IFP; and 0.02 , 6.9740×10^{-3} , 0.02 and 0.4918 ,
 292 respectively, during the ICP in this paper.

293 The three models were selected, first, as they are typical representatives in considering mass transfer,

带格式的: 制表位: 20 字符, 居中 + 38 字符, 右对齐

带格式的: 制表位: 20 字符, 居中 + 38 字符, 右对齐

294 aerodynamics, ~~and energy transfer, respectively~~; second~~ly~~ because their demand parameters are easy to
295 acquire, which are adaptive to be promoted; and third, as they have been ~~proved-proven~~ to be efficient in
296 saline lakes (Hamdani et al., 2018). These models were first calibrated and validated based on daily E
297 observations from 2014 to 2019 during ~~the different periods of the AN, IFP and ICP, respectively~~. The
298 root-mean-square error (RMSE) and goodness of fit (R^2) were used to evaluate the effectiveness of the
299 models. A model with high R^2 and low RMSE values was selected for lake E simulation during the AN,
300 IFP and ICP ~~periods~~.

301 **2.67. Statistical analysis**

302 Summer and autumn were taken as June to August and September to November, respectively. During
303 data analysis, we first divided the 30-min observed energy exchange flux and climate data from 2014 to
304 2019 by the AN, IFP, and ICP based on the calculated ice phenology. Hence, we obtained datasets of five
305 cycle years from the IFP in 2014 to the ICP in 2018 (Fig. S2). Second, we ~~calculated~~ the multiday
306 average 30-min ~~observed~~ energy exchange flux during the IFP and ICP in each year to evaluate the basic
307 statistical characteristics of the diurnal E and exchange flux. The daily energy exchange flux and climate
308 ~~data were calculated by averaging the 30-min observed data for each day were then calculated by~~
309 ~~averaging the 30-min data for each day, the daytime (nighttime) energy exchange flux and climate data~~
310 ~~were calculated by averaging the 30-min observed data of 8:00 am to 7:30 pm (8:00 pm to 7:30 am), and~~
311 ~~And~~ one-way ANOVA was performed to compare the difference in E and G between the IFP and ICP in
312 each year from 2014 to 2018. Third, to explore the key factor controlling lake E, partial least squares
313 regression and random forest methods were used to calculate the sensitivity coefficient
314 ~~(representing standing for~~ the regression coefficient of each variable, which means the amount of change
315 in E caused by the variation of per unit in the variable) and importance of R_n , WS, Δe , Pres, albedo, WD,
316 $T_a - T_s$, T_l , and ICR to E during the daytime and nighttime ~~of~~ IFP and ICP, respectively. ~~The two methods~~
317 ~~analyze the relationship between E and climate and environmental factors from linear and nonlinear~~
318 ~~processes, respectively, and have been widely used in the study of hydrological and ecological fields~~
319 ~~(Desai and Ouarda, 2021; Li et al., 2022; Sow et al., 2022).~~— Finally, three models were validated and
320 two models were selected to ~~severally~~ calculate the interannual E during the IFP and ICP from
321 2003 to 2017 (the available ice phenology exhibits a limited cycle year from 2003 to 2017). Four

322 controlled tests were then conducted to quantify the contribution of the variation in Ta, Ts, WS, and Rs
323 to lake E from 2003 to 2017. ~~The analysis of partial least squares regression, random forest methods, and~~
324 ~~E simulation, calibration and verification were conducted at the daily scale.~~ The partial least squares and
325 random forest analyses were conducted in R and the other analyses were conducted in MATLAB.

326 3. Results

327 3.1. Diurnal and seasonal characteristics of evaporation and the energy budget during the different 328 freeze–thaw periods

329 The average E, LE, G, H, and Rn values (average from 2014 to 2018) were 1.20 ± 0.09 mm/d, $68.01 \pm$
330 4.93 W/m², 192.18 ± 7.00 W/m², 16.25 ± 1.21 W/m² and 276.45 ± 3.32 W/m², respectively, during the
331 IFP; and 1.11 ± 0.20 mm/d, 63.15 ± 11.31 W/m², 79.23 ± 18.12 W/m², 4.68 ± 0.37 W/m² and $147.06 \pm$
332 14.23 W/m², respectively, during the ICP. The daytime E, LE, G, H and Rn values were notably lower
333 during the ICP than ~~these~~ during the IFP, except ~~for~~ E and LE in 2014 (Figs. 2 and 3; Table ~~S1S2~~). In
334 addition, the daily peak LE and E values typically occurred at approximately 12 pm during the IFP and
335 approximately 2 pm during the ICP, and exhibited an approximately two–hour lag during the IFP and a
336 four–hour lag during the ICP over G and Rn (Fig. 2). At night, although lower E (at an average rate of
337 0.81 ± 0.17 mm/d) and LE (46.02 ± 9.71 W/m²) levels occurred during the ICP than during the IFP (at
338 average rates of 0.94 ± 0.05 mm/d and 53.09 ± 2.94 W/m², respectively), E (LE) accounted for ~~42%–45%~~
339 and ~~41%–45%~~ of the total daily E during the IFP and ICP, respectively (Figs. 2 and 3; Table ~~S1S2~~).
340 ~~Regarding~~~~In regard to~~ G, a similar release rate was found during ~~the~~ IFP and ICP, but the heat release
341 time was longer during ~~the~~ ICP than ~~that~~ during ~~the~~ IFP (Fig. 2).

342 The daily E ranged from 1.96 to 2.34 mm/d during the IFP and from 1.57 to 2.71 mm/d during the ICP,
343 and the average E sum reached 593.37 ± 44.87 mm/yr during the IFP and 175.22 ± 45.98 mm/yr during
344 the ICP from 2014 to 2018 (Fig. 3; Fig. S2; Table ~~S1S2~~). This ~~suggests~~~~suggested~~ an average E sum of
345 77% during the IFP and 23% during the ICP throughout the cycle year from 2014 to 2018 (with a lake E
346 sum ranging from 719.45 to 798.55 mm/yr and an average value of 768.58 ± 28.73 mm/yr) (Fig. 3). In
347 terms of G, QHL initially released heat in autumn, which lasted until the lake was completely frozen,
348 after which heat was absorbed from the lake thawing period throughout the summer (Fig. S2; Fig. S3).

349 3.2. Response of evaporation to climatic factors during the different freeze–thaw periods

350 The key controlling factor of lake E was explored based on the daily observed energy exchange flux and
351 climate data (E, Rn, WS, Δe, Pres, albedo, WD, Ta–Ts, and Tl) and ICR during the IFP and ICP from
352 2014 to 2018. The Δe (with a sensitivity coefficient of 0.28 in the daytime and 0.22 in the nighttime, P <
353 0.05), WS (with a sensitivity coefficient of 0.54 in the daytime and 0.43 in the nighttime, P < 0.05) and
354 Pres (with a sensitivity coefficient of 0.26 in the daytime and 0.14 in the nighttime, P < 0.05) notably
355 increased E (Fig. 4), and the effect was greater in the daytime than ~~that~~ in the nighttime during the IFP
356 (Fig. 4). The Rn (with a sensitivity coefficient of 0.25 in the nighttime, P < 0.05), WS (with a sensitivity
357 coefficient of 0.30 in the daytime and 0.22 in the nighttime, P < 0.05), Ta–Ts (with a sensitivity coefficient
358 of 0.59 in the daytime and 0.39 in the nighttime, P < 0.05) and ICR (with a sensitivity coefficient of 0.20
359 in the daytime and 0.17 in the nighttime, P < 0.05) imposed a significant positive effect on E during the
360 ICP (Fig. 4). Similarly, the top five important factors calculated with the random forest method were WS,
361 Δe, Pres, WD, and Ts during the IFP and Ta–Ts, Ta, WS, Rn, and ICR during the ICP (Fig. S4). This
362 indicated~~s~~ that E of QHL ~~is was~~ mainly controlled by WS, Δe, and Pres during the IFP but ~~is was~~ driven
363 by Rn, Ta–Ts, WS, and ICR during the ICP.

364 3.3. Evaporation simulation and interannual variation

365 Three models (MT, AD, and JH) were calibrated and validated to evaluate the interannual variation in
366 QHL E from 2003 to 2017. In the case of model performance, the MT model based on molecular diffusion
367 performed the best in terms of E simulation during the IFP (with the largest R² and smallest RMSE values
368 of ~~0.77–79~~ and ~~0.8885~~, respectively), while the JH model based on energy exchange performed the best
369 during the ICP (with the largest R² and smallest RMSE values of ~~0.68–65~~ and ~~1.0702~~, respectively) (Figs.
370 S5 and S6). Thus, the interannual variation in QHL E from 2003 to 2017 was calculated with the MT
371 model during the IFP and with the JH model during the ICP (Fig. 5). From 2003 to 2017, although
372 ~~decrease in~~ Ta (at a rate of –0.01°C/yr), Pres (at a rate of –0.01 hPa/yr) and WS (at a rate of ~~–0.006–004~~
373 m/(s·yr)) ~~decreased~~, increases in Δe (at a rate of 0.01 hPa/yr) and Ts (at a rate of 0.001°C/yr) resulted in
374 an increase in E (at a rate of ~~1.49–62~~ mm/yr for the E sum) during the IFP (Figs. 5 and S7). Conversely,
375 ignoring the increases in Ta (at a rate of 0.04°C/yr) and Ta–Ts (at a rate of 0.04°C/yr), with decreasing
376 WS (at a rate of ~~–0.008–005~~ m/(s·yr)), E (at a rate of ~~–1.96–98~~ mm/yr for the E sum) decreased during

设置了格式: 非突出显示

设置了格式: 非突出显示

设置了格式: 非突出显示

377 the ICP, which resulted in an inapparent ~~decrease~~ decrease in E (at a rate of ~~-0.460,36~~ mm/yr for the E
378 sum) during the AN (Figs. 5 and S7).

379 4. Discussion

380 4.1. Lake evaporation during the ice-covered period

381 The results of this study highlight the important contribution of lake ice sublimation to the total amount
382 of lake E. Due to the low snow coverage of Qinghai Lake in winter (with a maximal snow coverage less
383 than 16% of the area of Qinghai Lake), evaporation and sublimation of lake ice and water are the ~~main~~
384 ~~major~~ sources of E during the ICP of 2013–2018 (Fig S8). ~~In liquid drops, E can be explained based on~~
385 ~~the coffee-stain effect in which the local diffusion-limited E rate diverges at the contact line (the border~~
386 ~~of the liquid drops) and outward flow from a given droplet replenishes the corner region if the droplet~~
387 ~~contact line remains fixed (Deegan et al., 1997 and 2000). Similarly, ice crystal E also starts at the contact~~
388 ~~line first and quickly recedes along sharp crystal edges (Nelson, 1998; Jambon-Puillet et al., 2018). Since~~
389 ~~the mass loss caused by E cannot be replaced, the occurrence of E at sharp points causes these points to~~
390 ~~successively retreat, resulting in self-similar smoothness (Jambon-Puillet et al., 2018).~~ The experimental
391 and simulation results of Jambon-Puillet et al. (2018) verified that the E rates of liquid droplets and ice
392 crystals remain the same under unchanged environmental conditions. In this study, the E rate of QHL
393 during the ICP ranged from 1.57 to 2.71 mm/d, approximately 0.73–1.38 times that of liquid water during
394 the IFP (Table S4S2), with similar results to those findings of liquid droplets and ice crystals. ~~_~~
395 ~~In practice, lake E varies diurnally, seasonally, and interannually with climatic and environmental~~
396 ~~changes, and the E rate varies considerably among lakes in different regions.~~ Few studies have examined
397 lake ice E during the ICP, and most studies have focused on polar sea ice and alpine snow packs (Froyland
398 et al., 2010; Froyland, 2013; Herrero et al., 2016; Christner et al., 2017; Lin et al., 2020). Observational
399 and modelling studies of Antarctic ice sheets or lakes have found that the monthly E rate of ice ranged
400 from –4.6 to 13 mm/month from June to September (Antarctic) (Froyland et al., 2010). In this study, we
401 found that ~~the~~ E sum ranges from 130.59 to 262.45 mm during the ICP (~~approximately 51.60 to 81.3~~
402 ~~mm/month, by multiplying the mean daily E of ICP by 30) from 2014 to 2018, which is higher than the~~
403 previous observations from Antarctic ice sheets or lakes. This may be because Antarctic ice sheets or

设置了格式: 非突出显示

设置了格式: 非突出显示

设置了格式: 非突出显示

404 lakes are located at high latitudes with low solar radiation and are therefore cooler from the surface to
405 greater depths with energy-limiting conditions for E (Persson et al., 2002). However, the lakes on the
406 QTP freeze seasonally, so most of these lakes can store a large amount of heat because of the high solar
407 radiation during the IFP (Fig. 6), which could lead to the observed E during the ICP (Huang et al., 2011
408 and 2016). Studies on surface E of a shallow thermokarst lake in the central QTP region have found that
409 E reaches up to 250 mm/yr during the ICP (Huang et al., 2016), which is close to our observed E levels
410 (130.59–262.45 mm/yr). Our results further showed that E of QHL accounted for 23% of the annual E
411 during the ICP. Wang et al. (2020) evaluated 75 large lakes on the QTP and demonstrated that the E of
412 these lakes in winter accounted for 12.3%–23.5% of the annual E, which suggests that E of these lakes
413 during the ICP was the same as that during the other seasons. Furthermore, considering that the area of
414 QHL is 4,432 km² (Li et al., 2016), the QHL releases 3.39 ± 0.13 km³ of water into the air every year,
415 which corresponds to the sum of the water for animal husbandry, industrial and domestic uses in Qinghai
416 Province (an average of 2014 to 2017) (Dong et al., 2021).

417 4.2. Responses of lake evaporation to salinity and climate change

418 Salinity greatly influences the E of saline lakes by changing both water
419 density and thermal properties, dissolved salt ions can reduce the free energy of water molecules, and
420 result in a higher boiling point and reduced saturated vapor pressure above saline lakes at a given water
421 temperature (Salhotra et al., 1987; Abdelrady, 2013; Mor et al., 2018). Therefore, an increase in the
422 salinity of a lake would decrease its E rate. For example, Lee (1927) compared the E of pure water with
423 that of saline lakes of different densities (salinity) in Nevada, USA, and found that when the
424 density (salinity) of water increased by 1%, the E of saline lakes decreased by 0.01% compared
425 with that of pure water. Similarly, Mor et al. (2018) found that the E rate in a diluted plume is nearly
426 three times larger than that in open lake in the Dead Sea. Thus, the thermodynamic concept of water
427 activity which is defined as the ratio of water vapor pressure on the surface of saline and fresh water at
428 the same temperature (the water activity of freshwater is 1, while in that of saline water is lower than 1,
429 and the higher the salinity is, the lower of the water activity in lakes) has been widely used in E
430 simulations of saline lakes, which is defined as the ratio of water vapor pressure on the surface of saline
431 and fresh water at a given temperature (Salhotra et al., 1987; Abdelrady, 2013; Mor et al., 2018). In our

432 study, we measured the water activity of QHL ~~was as~~ 0.97 by a salinity of 14.13 g L⁻¹, and applied it to
433 the ~~MT and AD~~ models ~~for E simulation of IFP during 2003 to 2017~~, which make it more theoretical to
434 explain ~~the E~~ process of saline lakes and reduced the uncertainty of estimation in saline lake E. For
435 example, with the salinity of 133 g L⁻¹ of surface water, water activity was measured to be 0.65~~3~~, and has
436 been widely used in its E simulation of ~~the Dead S~~sea (Metzger et al., 2018; Mor et al., 2018; Lensky et
437 al., 2018); and Abdelrady (2013) improved the surface energy balance system (SEBS) of E in saline lakes
438 by constructing an exponential function between lake salinity and water activity, which reduced the
439 simulated E by 27% and RMSE from 0.62 to 0.24 mm 3h⁻¹ in ~~the~~Great Salt Lake. Therefore, considering
440 salinity is ~~essential to enhance the accuracy of E simulations in saline lakes~~~~very important to improve~~
441 ~~the accuracy of E simulation in saline lakes. Certainly, lake salinity changes dynamically at diurnal,~~
442 ~~seasonal and interannual scales, but since the difficult of continuously observation of lake salinity, a fixed~~
443 ~~water activity in our study may cause the underestimate in E of QHL, due to the decrease of salinity by~~
444 ~~the expansion of QHL.~~

445 **4.3. Responses of lake evaporation to climate variability**

446 ~~Furthermore~~~~In addition~~, climate and environment are also important factors affecting lake E, and ~~varied~~
447 ~~vary~~ significantly ~~among-between~~ the different seasons. Previous studies have shown that lake E is
448 ~~mainly-mostly~~ affected by WS and Δe in summer and WS, Δe, Ta-Ts, and G in winter (Zhang and Liu,
449 2014; Hamdani, et al., 2018). This suggests that energy exchange between lakes and air may be one of
450 the main drivers of E during the ICP under the same atmospheric boundary conditions (Fig. 6). Since
451 most lakes store heat in summer, they release heat and sufficiently produce E in winter (Blanken et al.,
452 2011; Hamdani, et al., 2018). In this study, we also found that QHL began to store heat in the lake thawing
453 period and released heat in autumn or when the lake began to freeze (Figs. 6 and S3). Therefore, E of
454 QHL was ~~mainly-mostly~~ controlled by WS, Δe, and Pres during the IFP, whereas it was mainly affected
455 by Rn, Ta-Ts and WS during the ICP (Fig. 6).

456 ~~Furthermore, the QTP has been suffering~~ ~~Considering the overall~~ surface air warming and moistening,
457 solar dimming, and wind stilling since the beginning of the 1980s across the QTP (Yang et al., 2014;
458 ~~Kuang and Jiao, 2016~~), which affects the hydrothermal processes of the lake, such as increasing Ts and
459 ~~shortening lake ice phenology (Wan et al., 2018; Cai et al., 2019).~~ ~~An increase in Ts enhances the~~

设置了格式: 字体: 加粗
带格式的: 3 级, 与下段同页, 段中不分页

460 diffusion of water molecules and enlarges Δe between the water surface and the air, which in turn
461 promotes evaporation (Wang et al., 2018; Woolway et al., 2020), while a reduction in solar radiation
462 decreases the energy input of the lake, and wind stilling enhances the stability of the atmosphere above
463 the water surface, which in turn inhibits evaporation (Roderick and Farquhar, 2022; Guo et al., 2019).
464 We found a decrease in E during the AN from 2003 to 2017, due to the steeper decrease in E caused by
465 solar dimming and wind stilling during the ICP than the increase engendered by the increase in Ts during
466 the IFP. From 2003 to 2017, we further explored the contribution of Ta, Ts, WS and Rs to E during the
467 IF and IC from 2001 to 2017 by simulation tests. Compared with 2001, E during the IC increased at an
468 average rate (2003–2017) of 4.90 ± 6.14 mm/yr (3.52%) due to an increase in Ta and decreased at an
469 average rate (2003–2017) of -5.84 ± 3.54 mm/yr (3.37%), -6.48 ± 4.77 – 6.17 ± 4.77 mm/yr (3.4923%),
470 and -11.17 ± 14.29 – 18.92 ± 27.55 mm/yr (41.147.56%) due to an increase in Ts and decrease in Rs
471 and WS during the ICP, respectively (Fig. 7; Table S2S3), while, moreover, the increase in Ts increased
472 E at an average rate (2003–2017) of 13.58 ± 20.75 – 10.19 ± 19.00 mm/yr (3.3754%) during the IFP (Fig.
473 7; Table S2S3). Previous studies have found similar results in Selin Co and Namu Co (Zhu et al., 2016;
474 Guo et al., 2019). For example, Guo et al. (2019) found that E was mainly controlled by WS, and a
475 decrease in WS led to a decrease in E from 1985 to 2016 in Selin Co.

476 In addition, changes in lake ice phenology significantly affected lake E during the IFP and ICP. Compared
477 with 2003 to 2007 (101.40 \pm 7.00 d), the average ICP decreased by 10.8 d from 2013 to 2017 (90.60 \pm
478 6.08 d) (Table S3). A shortened ICP suggests a much lower albedo in the cycle year and could result in
479 higher Rs absorption and a shorter period for heat-induced recession, which could increase lake E (Wang
480 et al., 2018). Furthermore, of course, lake E is also affected by the lake area, water level, and physical and
481 chemical properties (Woolway et al., 2020), especially for saline lakes (Salhotra et al., 1987; Mohammed
482 and Tarboton, 2012; Mor et al., 2018). Increasing the water salinity could reduce E (Salhotra et al., 1987;
483 Mor et al., 2018) because the dissolved salt ions could reduce the free energy of water molecules (i.e.,
484 reduced water activity) and result in a lower saturated vapor pressure above saline lakes at a given water
485 temperature (Salhotra et al., 1987; Mor et al., 2018). However, the changes in lake physical and chemical
486 properties attributed to lake freezing increase the complexity of the underlying mechanism, simulation
487 of ice E and its response to climate change, and more studies are needed to further explore interactions
488 between the different factors.

4.34. Uncertainty Limitation

Based on six continuous year-round direct measurements of lake E and energy exchange flux, we determined the E loss during the ICP and calibrated and verified different models for E simulation during the IFP and ICP. Due to the lack of accurate measurements of deep lake temperatures, energy budget closure ratios of EC observations in QHL are not given in this study. EC measurements have been widely used to quantify the E of several global lakes, including Lake Superior in America, Great Slave ~~lake~~ Lake in Canada, Lake Geneva in Switzerland, Lake Valkea-Kotinen in Finland, and Taihu Lake, Erhai Lake, Poyang Lake, Nam Co, Selin Co and Ngoring Lake in China (Blanken et al., 2000; Vercauteren et al., 2009; Blanken et al., 2011; Nordbo et al., 2011; Wang et al., 2014; Li et al., 2015; Liu et al., 2015; Guo et al., 2016; Li et al., 2016; Ma et al., 2016; Lensky et al., 2018). With ~~the~~ most of the known energy budget closure ratios ~~is~~ over 0.7, EC observations of lakes ~~is~~ are regarded as an accurate and reliable direct measurement method of E, even in lakes over ~~the~~ QTP (Wang et al., 2020). ~~Moreover, Certainly,~~ compared with land stations, the energy budget closure ratios over lake surfaces can be significantly influenced by the large amount of heat storage (release) during different seasons (Wang et al., 2020), which would increase the uncertainty about the quantification of E. ~~In addition, Besides,~~ quantification of E during the ICP depends on accurate ice phenology identification, and a longer ICP suggests more E. Therefore, the different data sources and phenological classification methods of ice phenology comprise one source of uncertainty. ~~Moreover-In addition,~~ lake salinity changes dynamically at diurnal, seasonal and interannual scales, but due to the difficulty of continuously observing lake salinity, the fixed water activity in our study may cause the underestimation in E of QHL due to the decrease in salinity by the expansion of QHL. Furthermore, in addition to the traditional lake evaporation models (Dalton formula series, energy and water balance formula series, Penman formula series, and empirical formula based on statistical analysis), the 1D lake thermodynamics model has been widely used for the simulation of lake ice thickness and energy balance (ice sublimation) in ICP (Pour et al., 2017; Stepanenko et al., Xie et al., 2023). Considering that this study was concentrate on verifying the consistency of the accuracy of the traditional models for the evaporation simulation during IFP and ICP. Thus, this study ignored the 1D lake thermodynamics model for ice sublimation. It is significant to build the observation system of lake thermodynamics parameters, verify and develop a suitable 1D or even 3D lake thermodynamics evaporation models for QHL in future study.we examined the sensitivity of the input variables (T_a , T_s ,

518 *Rs and WS) of the chosen model. Increases in Ta, Ts, Rs, and WS of 10% could result in changes of*
519 *-2.25%, 1.78%, 10.00% and 10.00% in the simulated E during the IC, respectively, indicating that E is*
520 *more sensitive to Rs and WS than Ta and Ts in the JH model during the IC (Fig. S9). Moreover, the*
521 *simulated E is minimally sensitive to Ta, and a 10% increase in WS could result in a change of 8.54% in*
522 *the simulated E during the IF, while a change in Ts could lead to an exponential change in the simulated*
523 *E (Fig. S9).*

524 **5. Conclusions**

525 In summary, based on six continuous year-round 30-min direct flux measurements throughout the cycle
526 year from 2014 to 2018, the night E of QHL occupied over 40% during both the IFP and ICP. With a
527 multiyear average of 175.22 ± 45.98 mm/yr, E during the ICP accounted for 23% of the total cycle year
528 E sum, which is an important component in calculating the E of saline lakes. A difference-based control
529 factor of E was also found during the IFP and ICP. E of QHL was mainly controlled by atmospheric
530 dynamic factors (WS, Δe , and P) during the IFP, whereas it was driven by both energy exchange and
531 atmospheric boundary conditions (R_n , T_a - T_s and WS) during the ICP. Thus, the MT model based on
532 molecular diffusion performed best in lake E simulation during the IFP, while the JH model based on
533 energy exchange performed best during the ICP. Furthermore, simulation of the E of QHL showed a
534 slight decrease from 2003 to 2017, caused by a decrease in E during the ICP, and WS weakening may
535 have resulted in an average reduction of 11.1% in lake E during the ICP from 2003 to 2017. Our results
536 suggest that E during the ICP is non-negligible for saline lake E, and E simulation should be further
537 improved in future model simulation studies, considering the difference in its potential mechanisms
538 during the ICP.

539 **Author Contributions**

540 XY Li conceived the idea, and FZ Shi performed the analyses. XY Li, FZ Shi, DL Chen and YJ Ma led
541 the manuscript writing. SJ Zhao, YJ Ma, JQ Wei and QW Liao provided analysis of datasets. All authors
542 contributed to the review and the revision of the manuscript.

543 **Acknowledgements**

544 The study was financially supported by the National Natural Science Foundation of China

545 (NSFC: 41971029), the Second Tibetan Plateau Scientific Expedition and Research Program
546 (STEP, grant no. 2019QZKK0306), the State Key Laboratory of Earth Surface Processes and
547 Resource Ecology (2021–ZD–03) and ~~the~~ Ten Thousand Talent Program for ~~leading-Leading~~
548 ~~Y-young seientists-Scientists~~ and the China Scholarship Council. The gridded climate datasets
549 from the interim reanalysis dataset v5 (ERA5) produced by the European Centre for Medium–
550 Range Weather Forecasts (<https://cds.climate.copernicus.eu/cdsapp#!/search?type=dataset>) and
551 the China Regional High–Temporal–Resolution Surface Meteorological Elements–Driven
552 Dataset (CMFD) (<http://data.tpdc.ac.cn/en/>) can be freely accessed. The daily lake ice coverage
553 data were retrieved from the National Tibetan Plateau Data Center
554 (<https://doi.org/10.11922/sciencedb.744>~~http://data.tpdc.ac.cn/en/~~).

555 **Competing interests**

556 The contact author has declared that ~~none of~~ the authors ~~has~~ have no any competing interests.

557

558 **References**

559 Abdelrady, A. R. Evaporation over fresh and saline water using SEBS. 2013. Master's Thesis. University
560 of Twente.

561 Allen, R. G., Pereira, L. S., Raes, D., & Smith, M. (1998). Crop evapotranspiration—Guidelines for
562 computing crop water requirements—FAO Irrigation and drainage paper 56. Fao, Rome, 300(9), D05109.

563 [Badawy, S. M. \(2016\). Laboratory freezing desalination of seawater. *Desalination and Water Treatment*,
564 *57*\(24\), 11040-11047.](#)

565 Blanken, P. D., Black, T. A., Neumann, H. H., Den Hartog, G., Yang, P. C., Nestic, Z., ... & Novak, M. D.
566 (1998). Turbulent flux measurements above and below the overstory of a boreal aspen forest. *Boundary–*
567 *Layer Meteorology*, *89*(1), 109–140.

568 Blanken, P. D., Rouse, W. R., Culf, A. D., Spence, C., Boudreau, L. D., Jasper, J. N., ... & Verseghy, D.
569 2000. Eddy covariance measurements of evaporation from Great Slave lake, Northwest Territories,
570 Canada. *Water Resources Research*, *36*(4): 1069–1077.

571 Blanken, P. D., Spence, C., Hedstrom, N., & Lenters, J. D. (2011). Evaporation from Lake Superior: 1.
572 Physical controls and processes. *Journal of Great Lakes Research*, *37*(4), 707–716.

573 Bowen, I. S. (1926). The ratio of heat losses by conduction and by evaporation from any water surface.
574 *Physical Review*, *27*(6), 779.

575 Cai, Y., Ke, C. Q., Li, X., Zhang, G., Duan, Z., & Lee, H. (2019). Variations of lake ice phenology on the
576 Tibetan Plateau from 2001 to 2017 based on MODIS data. *Journal of Geophysical Research:*
577 *Atmospheres*, *124*(2), 825–843.

578 Christner, E., Kohler, M., & Schneider, M. (2017). The influence of snow sublimation and meltwater
579 evaporation on δD of water vapor in the atmospheric boundary layer of central Europe. *Atmospheric*
580 *Chemistry and Physics*, *17*(2), 1207–1225.

581 Dalton, J. (1802). Experimental essays on the constitution of mixed gases; on the force of stream or vapor
582 from water and other liquids, both in a Torricellian vacuum and in air; on evaporation; and on the
583 expansion of gases by heat. *Proceedings of Manchester Literary and Philosophical Society*, *5*, 536–602.

584 Deegan, R. D., Bakajin, O., Dupont, T. F., Huber, G., Nagel, S. R., & Witten, T. A. (1997). Capillary flow
585 as the cause of ring stains from dried liquid drops. *Nature*, *389*(6653), 827–829.

586 Deegan, R. D., Bakajin, O., Dupont, T. F., Huber, G., Nagel, S. R., & Witten, T. A. (2000). Contact line
587 deposits in an evaporating drop. *Physical review E*, *62*(1), 756.

588 [Desai, S., & Ouarda, T. B. M. J. \(2021\). Regional hydrological frequency analysis at ungauged sites with
589 random. *Journal of Hydrology*, *594*: 125861.](#)

590

591 Dong, H., Feng, Z., Yang, Y., Li, P., & You, Z. (2021). Sustainability assessment of critical natural capital:

592 a case study of water resources in Qinghai Province, China. *Journal of Cleaner Production*, 286, 125532.

593 Falge, E., Baldocchi, D., Olson, R., Anthoni, P., Aubinet, M., Bernhofer, C., ... & Wofsy, S. (2001). Gap
594 filling strategies for defensible annual sums of net ecosystem exchange. *Agricultural and forest*
595 *meteorology*, 107(1), 43–69.

596 Finch, J., & Calver, A. (2008). Methods for the quantification of evaporation from lakes. Prepared for
597 the World Meteorological Organization’s Commission for Hydrology, 1–41.

598 Froyland, H. K. (2013). Snow loss on the San Francisco peaks: Effects of an elevation gradient on evapo-
599 sublimation (Doctoral dissertation, Northern Arizona University).

600 Froyland, H. K., Untersteiner, N., Town, M. S., & Warren, S. G. (2010). Evaporation from Arctic sea ice
601 in summer during the International Geophysical Year, 1957–1958. *Journal of Geophysical Research:*
602 *Atmospheres*, 115(D15).

603 Gross, M. 2017. The world’s vanishing lakes. *Current Biology*, 27, 43–46. doi:
604 10.1016/j.cub.2017.01.008.

605 Guo, Y., Zhang, Y., Ma, N., Song, H., & Gao, H. (2016). Quantifying surface energy fluxes and
606 evaporation over a significant expanding endorheic lake in the central Tibetan Plateau. *Journal of the*
607 *Meteorological Society of Japan. Ser. II*, 94, 453–465.

608 Guo, Y., Zhang, Y., Ma, N., Xu, J., & Zhang, T. (2019). Long-term changes in evaporation over Siling
609 Co Lake on the Tibetan Plateau and its impact on recent rapid lake expansion. *Atmospheric research*, 216,
610 141–150.

611 Hamdani, I., Assouline, S., Tanny, J., Lensky, I. M., Gertman, I., Mor, Z., & Lensky, N. G. (2018).
612 Seasonal and diurnal evaporation from a deep hypersaline lake: The Dead Sea as a case study. *Journal of*
613 *Hydrology*, 562, 155–167.

614 [Han, W. X., Huang, C. L., Gu, J., Hou, J. L., & Zhang, Y. \(2021\). Spatial–Temporal Distribution of the](#)
615 [Freeze–Thaw Cycle of the Largest Lake \(Qinghai Lake\) in China Based on Machine Learning and](#)
616 [MODIS from 2000 to 2020. *Remote Sensing*, 13\(9\): 1695.](#)

617 Harbeck, G. E. (1958). Water-loss investigations: Lake Mead studies (Vol. 298). US Government
618 Printing Office.

619 Herrero, J., & Polo, M. J. (2016). Evaposublimation from the snow in the Mediterranean mountains of
620 Sierra Nevada (Spain). *The Cryosphere*, 10(6), 2981–2998.

621 Huang, L., Liu, J., Shao, Q., & Liu, R. (2011). Changing inland lakes responding to climate warming in
622 Northeastern Tibetan Plateau. *Climatic Change*, 109(3), 479–502.

623 Huang, W., Li, R., Han, H., Niu, F., Wu, Q., & Wang, W. (2016). Ice processes and surface ablation in a
624 shallow thermokarst lake in the central Qinghai–Tibetan Plateau. *Annals of Glaciology*, 57(71), 20–28.

625 Jambon–Puillet, E., Shahidzadeh, N., & Bonn, D. (2018). Singular sublimation of ice and snow crystals.
626 *Nature communications*, 9(1), 1–6.

627 [Jin, Z. D., An, Z. S., Yu, J. M., Li, F. C., & Zhang, F. \(2015\). Lake Qinghai sediment geochemistry linked](#)

628 [to hydroclimate variability since the last glacial. *Quaternary Science Reviews*, 122\(2015\): 63–73.](#)

629 [Kuang, X., and Jiao, J. J. \(2016\). Review on climate change on the Tibetan Plateau during the last half](#)

630 [century. *Journal of Geophysical Research*, 121, 3979–4007.](#)

631 [Lazhu, Yang, K., Wang, J., Lei, Y., Chen, Y., Zhu, L., ... & Qin, J. \(2016\). Quantifying evaporation and](#)

632 [its decadal change for Lake Nam Co, central Tibetan Plateau. *Journal of Geophysical Research:*](#)

633 [Atmospheres](#), 121(13), 7578–7591.

634 Lee C.H. 1927. Discussion of “Evaporation on reclamation projects” by IE Houk. *Transactions of the*

635 *American Society of Civil Engineers*, 90: 340–343.

636 Lensky, N. G., Lensky, I. M., Peretz, A., Gertman, I., Tanny, J., & Assouline, S. (2018). Diurnal Course

637 of evaporation from the dead sea in summer: A distinct double peak induced by solar radiation and night

638 sea breeze. *Water Resources Research*, 54(1), 150–160.

639 Li, B., Zhang, J., Yu, Z., Liang, Z., Chen, L., & Acharya, K. (2017). Climate change driven water budget

640 dynamics of a Tibetan inland lake. *Global and Planetary Change*, 150, 70–80.

641 Li, X. Y., Ma, Y. J., Huang, Y. M., Hu, X., Wu, X. C., Wang, P., ... & Liu, L. (2016). Evaporation and

642 surface energy budget over the largest high-altitude saline lake on the Qinghai-Tibet Plateau. *Journal of*

643 *Geophysical Research: Atmospheres*, 121(18), 10–470.

644 [Li, X. Y., Shi, F. Z., Ma, Y. J., Zhao, S. J., & Wei, J. Q. \(2022\). Significant winter CO₂ uptake by saline](#)

645 [lakes on the Qinghai-Tibet Plateau. *Global Change Biology*, 2022, 28\(6\): 2041–2052.](#)

646 Li, Z., Lyu, S., Ao, Y., Wen, L., Zhao, L., & Wang, S. 2015. Long-term energy flux and radiation balance

647 observations over lake Ngoring, Tibetan Plateau. *Atmospheric Research*, 155: 13–25.

648 Lin, Y., Cai, T., & Ju, C. (2020). Snow evaporation characteristics related to melting period in a forested

649 permafrost region. *Environmental Engineering & Management Journal (EEMJ)*, 19(3).

650 Liu, C., Zhu, L., Wang, J., Ju, J., Ma, Q., Qiao, B., ... & Kai, J. (2021). In-situ water quality investigation

651 of the lakes on the Tibetan Plateau. *Science Bulletin*. 66(17): 1727–1730.

652 <https://doi.org/10.1016/j.scib.2021.04.024>.

653 Liu, H., Feng, J., Sun, J., Wang, L., & Xu, A. (2015). Eddy covariance measurements of water vapor and

654 CO₂ fluxes above the Erhai Lake. *Science China Earth Sciences*, 58(3), 317–328.

655 Ma, N., Szilagyi, J., Niu, G. Y., Zhang, Y., Zhang, T., Wang, B., & Wu, Y. (2016). Evaporation variability

656 of Nam Co Lake in the Tibetan Plateau and its role in recent rapid lake expansion. *Journal of Hydrology*,

657 537, 27–35.

658 Messenger, M. L., Lehner, B., Grill, G., Nedeva, I., & Schmitt, O. (2016). Estimating the volume and age

659 of water stored in global lakes using a geo-statistical approach. *Nature communications*, 7(1), 1–11.

660 Mohammed, I. N., & Tarboton, D. G. (2012). An examination of the sensitivity of the Great Salt Lake to

661 changes in inputs. *Water Resources Research*, 48(11).

662 Mor, Z., Assouline, S., Tanny, J., Lensky, I. M., & Lensky, N. G. (2018). Effect of water surface salinity

663 on evaporation: The case of a diluted buoyant plume over the Dead Sea. *Water Resources Research*, 54(3),

设置了格式: 下标

664 1460–1475.

665 Nelson, J. (1998). Sublimation of ice crystals. *Journal of the atmospheric sciences*, 55(5), 910–919.

666 Nordbo, A., Launiainen, S., Mammarella, I., Leppäranta, M., Huotari, J., Ojala, A., & Vesala, T. 2011.

667 Long-term energy flux measurements and energy balance over a small boreal lake using eddy covariance

668 technique. *Journal of Geophysical Research: Atmospheres*, 116: D02119.

669 [Obianyo, J. I. \(2019\). Effect of Salinity on Evaporation and the Water Cycle. *Emerging Science Journal*,](#)

670 [3\(4\): 256–262.](#)

671 Persson, P. O. G., Fairall, C. W., Andreas, E. L., Guest, P. S., & Perovich, D. K. (2002). Measurements

672 near the Atmospheric Surface Flux Group tower at SHEBA: Near-surface conditions and surface energy

673 budget. *Journal of Geophysical Research: Oceans*, 107(C10), SHE–21.

674 Penman, H. L. (1948). Natural evaporation from open water, bare soil and grass. *Proceedings of the*

675 *Royal Society of London. Series A. Mathematical and Physical Sciences*, 193(1032), 120–145.

676 [Pour, H. K., Duguay, C. R., Scott, K. A., & Kang, K. K. \(2017\). Improvement of lake ice thickness](#)

677 [retrieval from MODIS satellite data using a thermodynamic model. *IEEE Transactions on Geoscience*](#)

678 [and Remote Sensing](#), 55(10), 5956–5965.

679 Qiu, Y., Xie, P., Leppäranta, M., Wang, X., Lemmetyinen, J., Lin, H., & Shi, L. (2019). MODIS-based

680 daily lake ice extent and coverage dataset for Tibetan Plateau. *Big Earth Data*, 3(2), 170–185.

681 [Roderick M.L. & Farquhar, G.D. \(2022\). The cause of decreased pan evaporation over the past 50 years.](#)

682 [*Science* 298, 1410–1411.](#)

683 [Salhotra, A. M., Adams, E. E., & Harleman, D. R. \(1985\). Effect of Salinity and Ionic Composition on](#)

684 [Evaporation: Analysis of Dead Sea Evaporation Pans. *Water Resources Research*, 21\(9\), 1336–1344.](#)

685 Salhotra, A. M., Adams, E. E., & Harleman, D. R. (1987). The alpha, beta, gamma of evaporation from

686 saline water bodies. *Water Resources Research*, 23(9), 1769–1774.

687 [Sow, A., Traore, I., Diallo, T., Traore, M., & Ba, A. \(2022\). Comparison of Gaussian process regression,](#)

688 [partial least squares, random forest and support vector machines for a near infrared calibration of](#)

689 [paracetamol samples. *Results in Chemistry*, 4: 100508.](#)

690 [Stepanenko, V. M., Repina, I. A., Ganbat, G., & Davaa, G. \(2019\). Numerical simulation of ice cover of](#)

691 [saline lakes. *Izvestiya, Atmospheric and Oceanic Physics*, 55, 129–138.](#)

692 [Su, D. S., Hu, X. Q., Wen, L. J., Lyu, S. H., Gao, X. Q., Zhao, L., ... & Kirillin, G. \(2019\). Numerical](#)

693 [study on the response of the largest lake in China to climate change. *Hydrology and Earth System*](#)

694 [Sciences](#), 23: 2093–2109.

695 [Tang, L. Y., Duan, X. F., Kong, F. J., Zhang, F., Zheng, Y. F., Li, Z., ... & Hu, S. J. \(2018\). Influences of](#)

696 [climate change on area variation of Qinghai Lake on Qinghai–Tibetan Plateau since 1980s. *Scientific*](#)

697 [Report](#), 8: 7331–7338.

698

699 Tian, W., Liu, X., Wang, K., Bai, P., & Liu, C. (2021). Estimation of reservoir evaporation losses for

-
- 700 China. *Journal of Hydrology*, 596, 126142.
- 701 Vercauteren, N., Bou-Zeid, E., Huwald, H., Parlange, M. B., & Brutsaert, W. 2009. Estimation of wet
702 surface evaporation from sensible heat flux measurements. *Water Resources Research*, 45(6): W06424.
- 703 Wan, W., Zhao, L., Xie, H., Liu, B., Li, H., Cui, Y., ... & Hong, Y. (2018). Lake surface water temperature
704 change over the Tibetan plateau from 2001 to 2015: A sensitive indicator of the warming climate.
705 *Geophysical Research Letters*, 45(20), 11–177.
- 706 Wang, B., Ma, Y., Chen, X., Ma, W., Su, Z., & Menenti, M. (2015). Observation and simulation of lake-
707 air heat and water transfer processes in a high-altitude shallow lake on the Tibetan Plateau. *Journal of*
708 *Geophysical Research: Atmospheres*, 120(24), 12327–12344.
- 709 Wang, B., Ma, Y., Wang, Y., Su, Z., & Ma, W. (2019a). Significant differences exist in lake-atmosphere
710 interactions and the evaporation rates of high-elevation small and large lakes. *Journal of hydrology*, 573,
711 220–234.
- 712 Wang, B., Ma, Y., Ma, W., Su, B., & Dong, X. (2019b). Evaluation of ten methods for estimating
713 evaporation in a small high-elevation lake on the Tibetan Plateau. *Theoretical and applied climatology*,
714 136(3), 1033–1045.
- 715 Wang, B., Ma, Y., Su, Z., Wang, Y., & Ma, W. (2020). Quantifying the evaporation amounts of 75 high-
716 elevation large dimictic lakes on the Tibetan Plateau. *Science advances*, 6(26), eaay8558.
- 717 Wang, W., Lee, X., Xiao, W., Liu, S., Schultz, N., Wang, Y., ... & Zhao, L. (2018). Global lake evaporation
718 accelerated by changes in surface energy allocation in a warmer climate. *Nature Geoscience*, 11(6), 410–
719 414.
- 720 Wang, W., Xiao, W., Cao, C., Gao, Z., Hu, Z., Liu, S., ... & Lee, X. 2014. Temporal and spatial variations
721 in radiation and energy balance across a large freshwater lake in China. *Journal of Hydrology*, 511:
722 811–824.
- 723 Woolway, R. I., Kraemer, B. M., Lenters, J. D., Merchant, C. J., O'Reilly, C. M., & Sharma, S. (2020).
724 Global lake responses to climate change. *Nature Reviews Earth & Environment*, 1(8), 388–403.
725 <https://doi.org/10.1038/s43017-020-0067-5>.
- 726 Woolway, R. I., Verburg, P., Lenters, J. D., Merchant, C. J., Hamilton, D. P., Brookes, J., ... & Jones, I.
727 D. (2018). Geographic and temporal variations in turbulent heat loss from lakes: A global analysis across
728 45 lakes. *Limnology and Oceanography*, 63(6), 2436–2449.
- 729 Wu, H., Huang, Q., Fu, C., Song, F., Liu, J., & Li, J. (2021). Stable isotope signatures of river and lake
730 water from Poyang Lake, China: Implications for river-lake interactions. *Journal of Hydrology*, 592,
731 125619.
- 732 Wu, H., Song, F., Li, J., Zhou, Y., Zhang, J., & Fu, C. (2022). Surface water isoscapes ($\delta^{18}\text{O}$ and $\delta^2\text{H}$)
733 reveal dual effects of damming and drought on the Yangtze River water cycles. *Journal of Hydrology*,
734 610, 127847.
- 735 Wurtsbaugh, W. A., Miller, C., Null, S. E., DeRose, R. J., Wilcock, P., Hahnenberger, M., ... & Moore, J.
736 (2017). Decline of the world's saline lakes. *Nature Geoscience*, 10(11), 816–821.

-
- 737 Xiao, M., & Cui, Y. (2021). Source of evaporation for the seasonal precipitation in the Pearl River Delta,
738 China. *Water Resources Research*, e2020WR028564.
- 739 [Xie, F., Lu, P., Leppäranta, M., Cheng, B., Li, Z., Zhang, Y., ... & Zhou, J. \(2023\). Heat budget of lake
740 ice during a complete seasonal cycle in lake Hanzhang, northeast China. *Journal of Hydrology*, 620,
741 129461.](#)
- 742 Yang, K., Hou, J., Wang, J., Lei, Y., Zhu, L., Chen, Y., ... & He, X. (2021). A new finding on the
743 prevalence of rapid water warming during lake ice melting on the Tibetan Plateau. *Science Bulletin*.
- 744 Yang, K., Wu, H., Qin, J., Lin, C., Tang, W., & Chen, Y. (2014). Recent climate changes over the Tibetan
745 Plateau and their impacts on energy and water cycle: A review. *Global and Planetary Change*, 112, 79–
746 91.
- 747 Zhang, Q., & Liu, H. (2014). Seasonal changes in physical processes controlling evaporation over inland
748 water. *Journal of Geophysical Research: Atmospheres*, 119(16), 9779–979.
- 749 [Zhu, L., Yang, K., Wang, J., Lei, Y., Chen, Y., Zhu, L., ... & Qin, J. \(2016\). Quantifying evaporation and
750 its decadal change for Lake Nam Co, central Tibetan Plateau. *Journal of Geophysical Research:
751 Atmospheres*, 121\(13\), 7578–7591.](#)

752 **Figure Legends**

753 **Figure 1. Location of Qinghai Lake (below) and the measurement site of the Chinese Torpedo**
754 **Qinghai Lake test base (upper).** The insets in the upper picture are photos of the four-way radiometer
755 and infrared thermometer (left), meteorological variable measurements (middle), and eddy covariance
756 sensors (right). [The scale is just for the Qinghai Lake Basin.](#)

757 **Figure 2. Diurnal characteristics of evaporation (E), latent heat flux (LE), sensible heat flux (H),**
758 **heat storage change (G) and net radiation (Rn) of Qinghai Lake (QHL) during the ice-free (IF)**
759 **and ice-covered (IC) periods (IFP and ICP) from 2014 to 2018.** The multiday average 30-min data
760 during the IFP and ICP in each cycle year are shown here, and the colored shading indicates a 0.5 standard
761 deviation. The gray area indicates nighttime. The labels 2014/2015, 2015/2016, 2016/2017, 2017/2018
762 and 2018/2019 indicate the cycle year of the freeze-thaw cycles.

763 **Figure 3. Evaporation (E) rate (a, c, and e) and annual E sum (b, d and f) of Qinghai Lake (QHL)**
764 **during the cycle year (annual: AN), ice-free (IF) and ice-covered (IC) periods (IFP and ICP) in**
765 **each cycle year from 2014 to 2018.** a and b show daily data, c and d show daytime data, and e and f
766 show nighttime data. The whiskers in a, c and e show the 1.5 interquartile range, while the letter
767 associated with the whiskers indicates statistically significant differences via one-way ANOVA during
768 the different freeze-thaw periods in each year from 2014 to 2018. The labels 2014/2015, 2015/2016,
769 2016/2017, 2017/2018, and 2018/2019 indicate the cycle year of freeze-thaw cycling.

770 **Figure 4. Sensitivity coefficient between the daytime and nighttime climatic factors and**
771 **evaporation (E) rate of Qinghai Lake (QHL) during the ice-free (IF) and ice-covered (IC) periods**
772 **(IFP and ICP).** *, ** and *** indicate statistical significance at the $P < 0.1$, $P < 0.05$ and $P < 0.01$ levels,
773 respectively, via Student's t tests. Rn, Δe , WS, WD, Pres, Ta-Ts, Tl and ICR indicate the net radiation,
774 vapor pressure difference, wind speed, wind direction, Pres, the difference between the air and lake
775 surface temperatures, the average temperature of the lake body from 0 to 300 cm, and ice coverage rate,
776 respectively.

777 **Figure 5. Interannual variability in the simulated evaporation (E) rate (a-c) and annual E sum**
778 **(d-f) of Qinghai Lake (QHL) in the cycle year (annual: AN), ice-free (IF), and ice-covered (IC)**

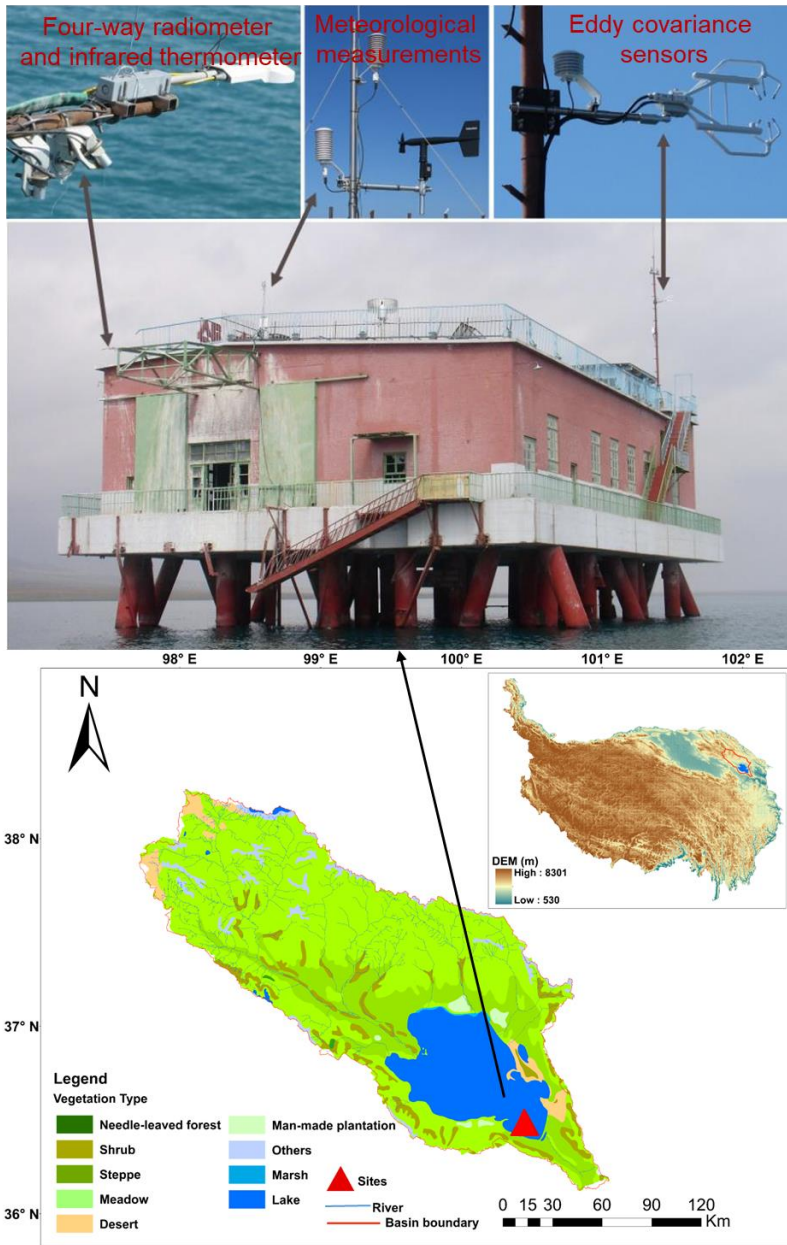
779 periods **(IFP and ICP)** from 2003 to 2017. The blue shading indicates a 0.5 standard deviation, and the
780 red shading indicates the 95% confidence interval of the trend line.

781 **Figure 6. Evaporation (E) and heat storage change (G) in Qinghai Lake (QHL) during the ice-free**
782 **~~(HF)~~ and ice-covered ~~(HC)~~ periods (IFP and ICP).** WS, Pres, Δe , $T_a - T_s$, R_n , and ICR are the wind
783 speed, air pressure, vapor pressure difference, difference between T_a and T_s , net radiation, and ice
784 coverage rate of the lake, respectively. The red plus sign indicates a positive effect of the variable on E.

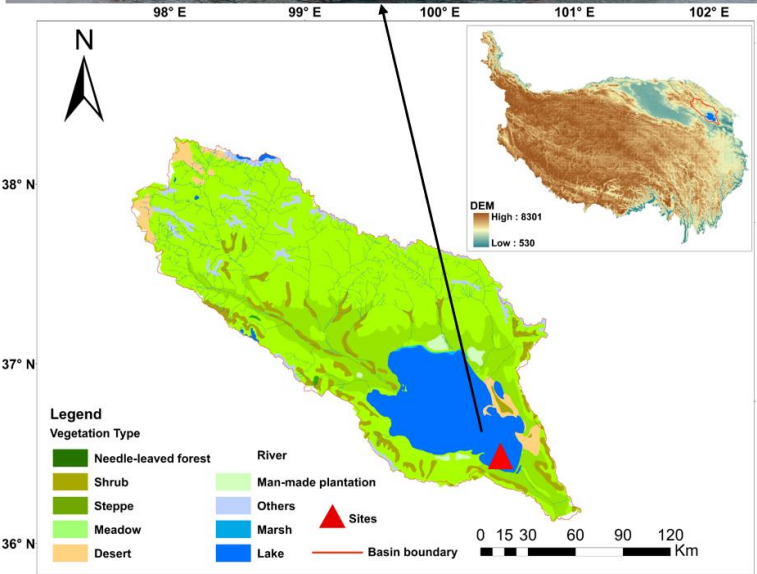
785 **Figure 7. The multiyear average contribution of the changes in air temperature (T_a), lake surface**
786 **temperature (T_s), downward shortwave radiation (Rs), and wind speed (WS) to the simulated**
787 **evaporation (E) of Qinghai Lake (QHL) in the cycle year (annual: AN), ice-free ~~(HF)~~ and ice-**
788 **covered ~~(HC)~~ periods (IFP and ICP) from 2003 to 2017.** a shows the multiyear average change in the
789 E rate caused by T_a , T_s , Rs, and WS; b shows the multiyear average change in the annual E sum caused
790 by T_a , T_s , Rs, and WS; and c shows the multiyear average change percentage of E caused by T_a , T_s , Rs,
791 and WS. The whiskers indicate a 0.5 standard deviation.

792 **Figures**

793 **Figure 1.**

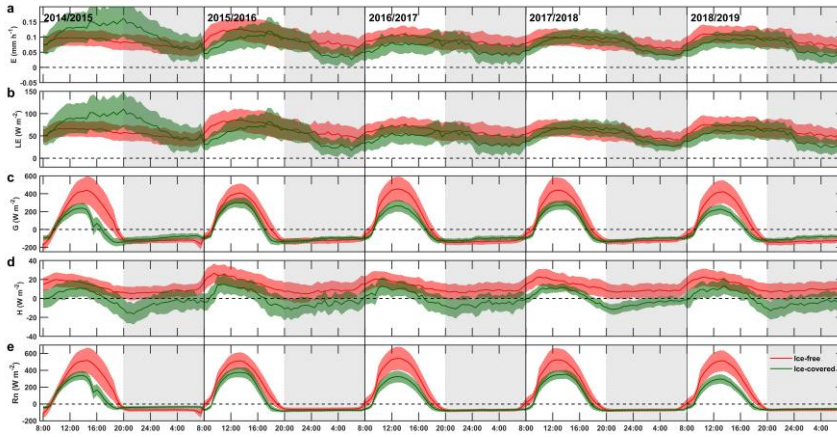


794



795

796 **Figure 2.**

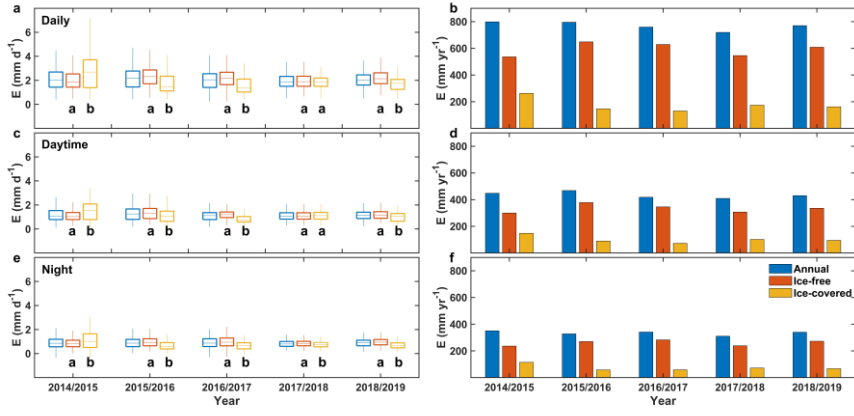


797

798

799

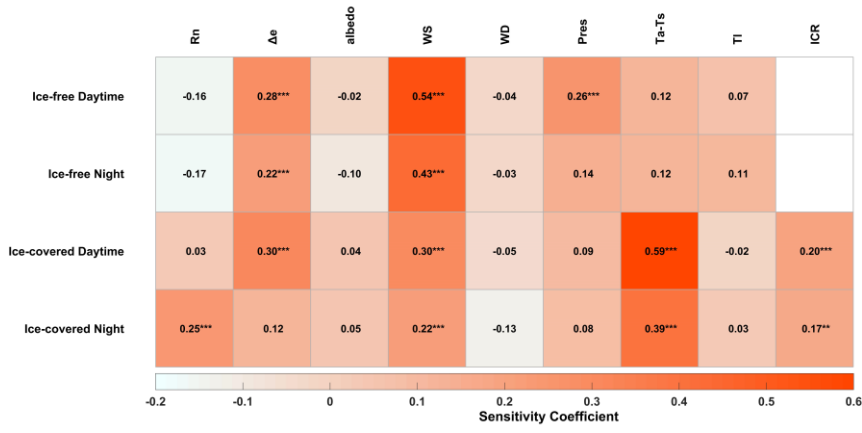
800 **Figure 3.**



801

802

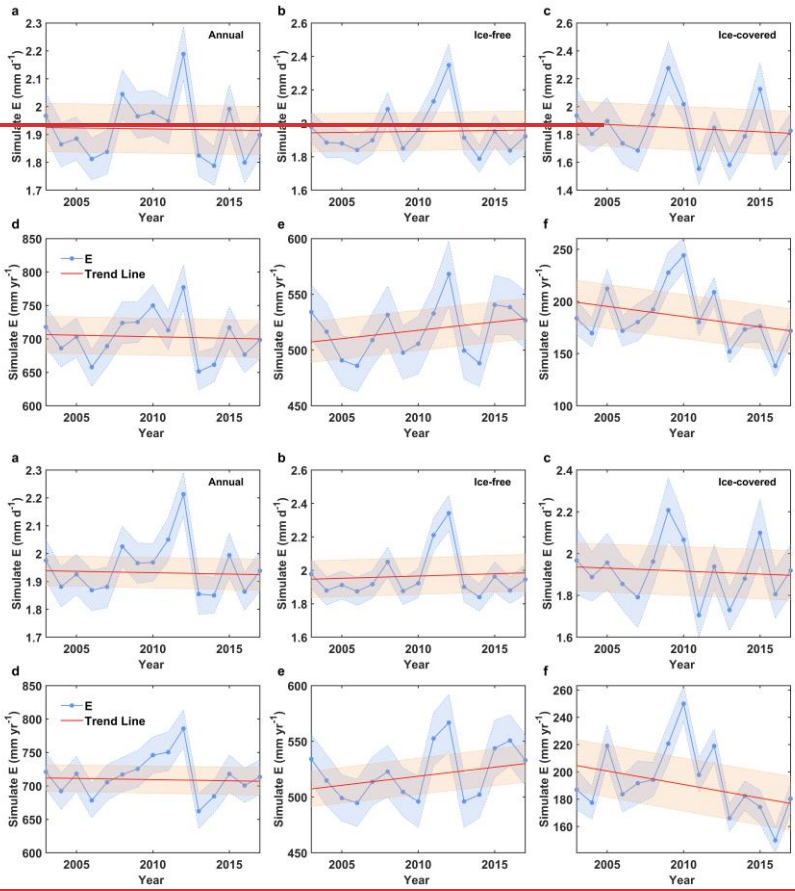
803 **Figure 4.**



804

805

806 **Figure 5.**

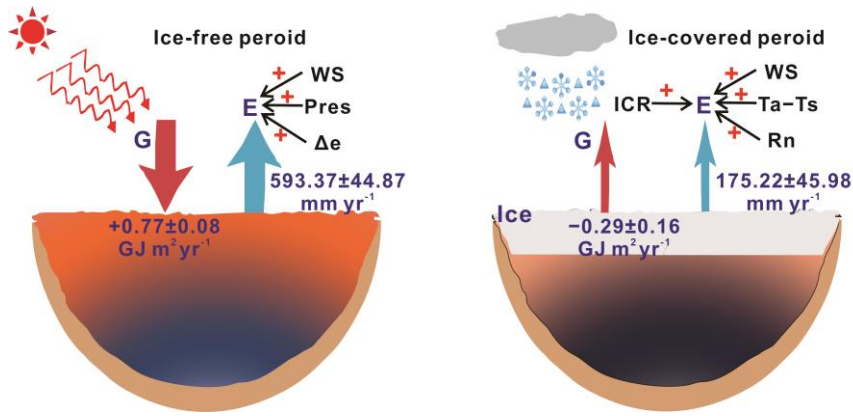


807

808

809

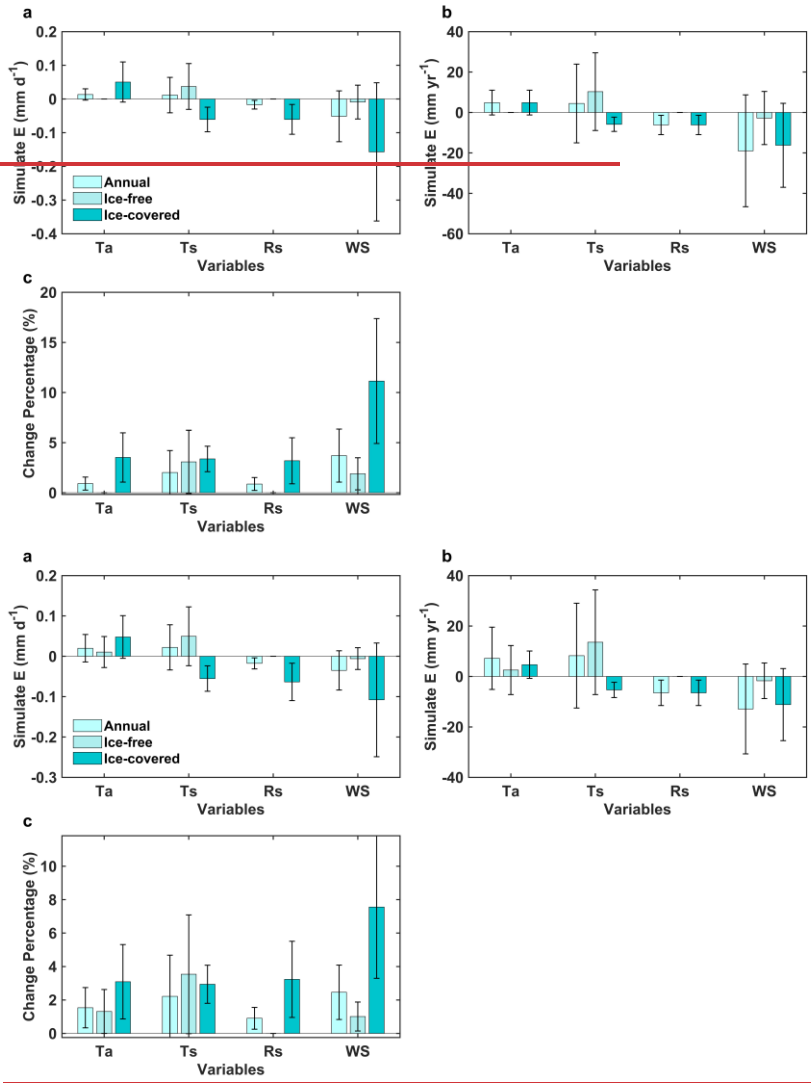
810 **Figure 6.**



811

812

813 **Figure 7.**



814

815

816